IEEE Access
Multidisciplinary | Rapid Review | Open Access Journal

Received April 13, 2019, accepted July 17, 2019, date of current version January 3, 2020.

Digital Object Identifier 10.1109/ACCESS.2019.2935260

Frequency-Based Modeling of a Vehicle Fitted With Roll-Plane Hydraulically Interconnected Suspension for Ride Comfort and Experimental Validation

MING WANG[1], BANGJI ZHANG[1], YUANCHANG CHEN[2], NONG ZHANG[3], AND JIE ZHANG[1]

[1]State Key Laboratory of Advanced Design and Manufacture for Vehicle Body, Hunan University, Changsha 410082, China
[2]Structural Dynamics and Acoustic Systems Laboratory, University of Massachusetts at Lowell, Lowell, MA 01854, USA
[3]School of Automotive and Transportation Engineering, Hefei University of Technology, Hefei 230009, China

Corresponding author: Bangji Zhang (bangjizhang@hnu.edu.cn)

This work was supported in part by the National Natural Science Foundation of China under Grant 5187051675, and in part by the Natural Science Foundation of Hunan Provincial under Grant 2017JJ2031.

ABSTRACT A frequency-based modeling approach has been developed for the vehicle fitted with Hydraulically Interconnected Suspension (HIS) system. This frequency-based model has fewer degrees of freedom (DOF) than the reference time-based model. Several physical parameters of HIS system are selected to analytically investigate their effects on several indicators of vehicle roll, pitch and bounce modes, such as roll and pitch angular acceleration, vertical acceleration, and tire ground force. The HIS system parameters are also coordinately tuned and optimized to meet the ride comfort requirement. The full vehicle drop test is conducted for the experimental validation. The analytical results of the proposed model have a good agreement with the measurements.

INDEX TERMS Vehicle suspension, ride comfort, hydraulically interconnected suspension, frequency-based modelling, parameter tuning, experimental validation.

I. INTRODUCTION

Automotive suspension systems are important for vehicle handling stability and Noise, Vibration, and Harshness (NVH) behavior [1]. Active suspension control strategies have been used on luxury vehicles due to its easy integration with the programmable controller units [2], [3]. The active controller, however, is not an affordable configuration for most of the commercial cars.

The passive suspension systems, such as Hydraulically Interconnected Suspension (HIS) systems and their derivatives, still have a wide application in the heavy machinery, automotive, etc. Within a HIS system, hydraulic cylinders are installed close to the conventional suspensions. Usually, these cylinders are interconnected using pipes or hoses to meet certain functions, such as improving roll, pitch or vertical dynamic performance by adjusting the accumulators and valves to stiffness and damping control [4] for certain vibration modes [5]–[7]. The HIS systems can partially decouple the vibration modes of a vehicle body.

In early studies, the hydraulic cylinders were separately used on the vehicles and were modeled as a spring-damper element. Du and Zhang [8] modeled the hydraulic actuator as a spring device. Then, the interconnection concept had been introduced into the design of hydraulic suspensions. Cao *et al.* [9], [10] studied the connections between the upper and lower chambers of hydraulic cylinders. Zhang *et al.* [5] presented an innovative HIS system with air stored in the accumulators instead of the fluid cylinders. This configuration significantly enhanced the reliability of hydraulic suspensions. Also, for the first time, Zhang proposed a frequency-domain model of the HIS system. Then Smith *et al.* [6] studied the frequency-domain characteristics on a half-car test rig under different precharged fluid pressure in the HIS system circuits. The handling performance of the vehicle with the HIS system under

The associate editor coordinating the review of this article and approving it for publication was Bora Onat.

fishhook maneuver was also simulated. Ding *et al.* [11] extended the application of the HIS system to tri-axle trucks in which the HIS system was modeled by transfer matrices method. The impedance transformation matrix method was used to derive the hydraulic strut forces in pitch-resistant HIS system [12]. Zhang *et al.* [13] overcame the trade-off between the ride comfort and handling performance of a mining vehicle by adjusting the suspension stiffness or damping parameters through active control methods. Wu *et al.* [14] developed a kinetic dynamic suspension to achieve enhanced cooperative control of the roll and warp motion modes for on-road and off-road vehicles. Liu *et al.* [15] integrated the HIS model with a traditional tractor-semitrailer suspension. Qi *et al.* [16] proposed a new roll-plane HIS to enhance both roll and lateral dynamics of a two-axle bus. Tan *et al.* [17] developed a pitch-roll-interconnected hydro-pneumatic suspension system to achieve the resistance control for pitch, roll and bounce modes of ambulances to improve the stability and attenuate the vibration for the lying patients.

The existing studies mainly focus on the dynamic characteristics of the vehicle with HIS and the control strategies to improve the system performances. The mechanical-hydraulic coupled vehicle systems are modeled either in time-domain [10], [18] or in frequency-domain [5], [11]. However, some studies developed a large-scale system model, which is not computationally efficient and the size of the model should be reduced [19], [20]. While, some studies built a half vehicle model or a quarter vehicle model, which cannot well describe the dynamic behaviors of the full vehicle because HIS is usually designed for the full vehicle.

Also, the determination of the physical parameters of the system model is also important for the effectiveness of the developed model [21], [22]. The parameters identified from the parameter estimation might not well represent the real vehicle. The accuracy of the model is highly dependent on the extracted parameters from the measurement. However, the influence of the physical parameters on vehicle performance has not been comprehensively investigated.

To address these issues, a condensed full vehicle model coupled with HIS system is developed in the frequency domain. Then, the vehicle fitted with HIS is compared with the reference vehicle. The influence of the variation of model parameters on the vehicle performance, like ride comfort, is also investigated. Measurements are usually used as a reliable tool to assess and study the proposed dynamic model [23]–[26], especially the field testing [16]. A full vehicle drop-test is performed to validate the proposed frequency-based vehicle model.

II. FREQUENCY-BASED MODELLING OF THE VEHICLE SYSTEM

A. VEHICLE MODEL

Instead of using a finite element modeling approach [27]–[29], a rigid 7-DOF vehicle multibody model is built which is coupled with the HIS system, as shown in Fig.1, which includes vertical displacement in center of gravity (CG) of the

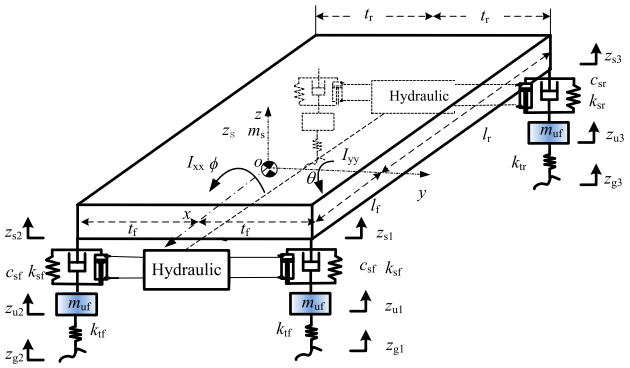

FIGURE 1. Vehicle model coupled with HIS system.

body z_s, roll angle ϕ, pitch angle θ and vertical displacements in the center of four wheels z_{ui} (i = 1,2,3,4). z_{si} (i = 1,2,3,4) denote the vertical displacements at four suspension stations, and they are dependent on the vehicle body motion. z_{gi} (i = 1,2,3,4) denote tire deflections caused by road roughness [30]–[32].

The state variables $\boldsymbol{X}$ of the vehicle model are defined as:

$$\boldsymbol{X} = \left[z_s \ \phi \ \theta \ z_{u1} \ z_{u2} \ z_{u3} \ z_{u4} \right] \tag{1}$$

Based on Newton's Second Law, the vehicle motion equations can be established as:

$$\boldsymbol{M}\ddot{\boldsymbol{X}}(t) + \boldsymbol{C}\dot{\boldsymbol{X}}(t) + \boldsymbol{K}\boldsymbol{X}(t) = \boldsymbol{F}(t) \tag{2}$$

where $\boldsymbol{M}$, $\boldsymbol{C}$, and $\boldsymbol{K}$ are system mass, damping and stiffness matrices, respectively. The values of the parameters of the vehicle are listed in the Appendix. $\boldsymbol{F}(t)$ denotes the forces generated by the tire deflections and applied on the vehicle unsprung mass [33], [34], which is defined as:

$$\boldsymbol{F}(t) = \boldsymbol{T}_{F\leftarrow Z}\boldsymbol{Z}_g(t) \tag{3}$$

where $\boldsymbol{T}_{F\leftarrow Z} = \left[\boldsymbol{0} \ \boldsymbol{K}_t^T \right]^T$ is the transfer function between the road excitation and the tire ground force. $\boldsymbol{K}_t = \mathrm{diag}([k_{tf}, k_{tf}, k_{tr}, k_{tr};])$.

The transfer function from external tire force input to the state variables can be defined as:

$$\boldsymbol{H}(s) = s^2\boldsymbol{M} + s\boldsymbol{C} + \boldsymbol{K} \tag{4}$$

Modal analysis [4], [35]–[36] is performed on the vehicle model and the modal parameters $s = \alpha + \mathrm{j}\beta$ is obtained and shown in Fig.2(a). α and β are the real and imaginary parts of s, respectively. The value s at each peak in Fig2(a) can also be expressed as $s = \varsigma\omega_n \pm j\omega_d$, ζ, ω_n and $\omega_d = \sqrt{1-\varsigma^2}\omega_n$ are the damping ratio, undamp-ed and damped natural frequency, respectively. Thus, the modal parameters can be obtained:

$$\omega_n = \sqrt{\alpha^2+\beta^2}, \quad \varsigma = \alpha/\omega_n, \ \omega_d = \beta \tag{5}$$

Then by solving the equation $(s\boldsymbol{I} - \boldsymbol{H}(s))\boldsymbol{X} = 0$, the eigenvector of each mode can be obtained. However, these eigenvectors, namely mode shapes, can be normalized by

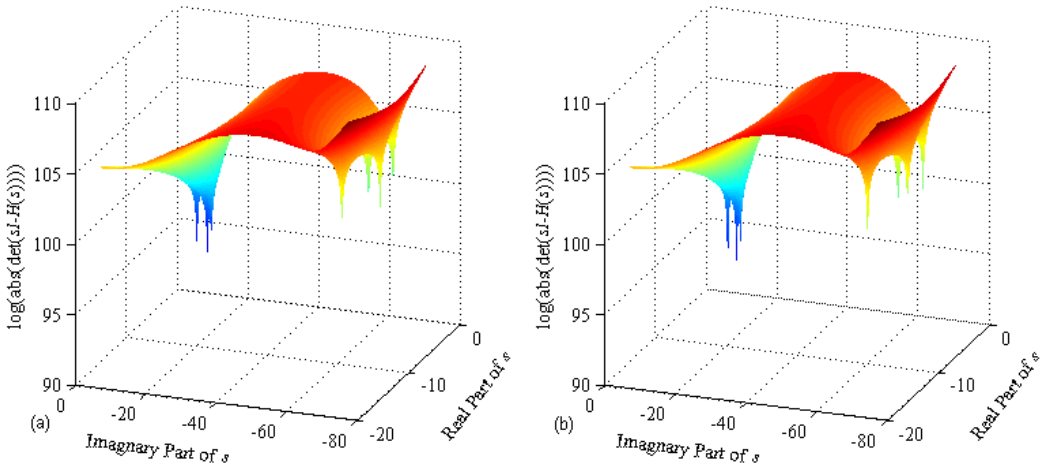

FIGURE 2. The transfer function H(s) of the vehicle model (a) vehicle only with conventional suspension; (b) vehicle with both conventional suspension and HIS system.

TABLE 1. Motion mode frequencies and shapes for a vehicle with/without HIS system.

A vehicle with only conventional suspension	Roll	Pitch	Bounce	Front wheel synchronized	Front wheel asynchronized	Rear wheel synchronized	Rear wheel asynchronized
Eigenvalue (λ_n)	-1.7336±5.7623i	-3.4878±8.2850i	-2.0244±7.1339i	-37.1606±62.9255i	-7.8174±69.4216i	-35.8672±62.9255i	-6.6860±69.3972i
Damped natural frequency (Hz) and damping ratio	f_n=0.917; ζ_n=0.288;	f_n=1.319; ζ_n=0.388;	f_n=1.135; ζ_n=0.273;	f_n=10.015; ζ_n=0.509;	f_n=11.049; ζ_n=0.112;	f_n=10.015; ζ_n=0.495;	f_n=11.045; ζ_n=0.096;
Sprung mass vertical motion (z_s)	-0.000 + 0.000i	0.452 + 0.061i	1	-0.032 - 0.043i	-0.000 - 0.000i	-0.014 - 0.048i	-0.000 - 0.000i
Sprung mass roll motion (ϕ)	1	-0.000 - 0.000i	0.000 + 0.000i	-0.000 + 0.000i	0.001 - 0.034i	-0.000 + 0.000i	-0.014 - 0.030i
Sprung mass pitch motion (θ)	0.000 - 0.000i	1	-0.307 - 0.037i	0.013 + 0.041i	0.000 - 0.000i	-0.028 - 0.051i	0.000 - 0.000i
Front left wheel vertical motion (z_{u1})	0.016 + 0.011i	-0.049 - 0.060i	0.109 + 0.110i	1	1	0.003 + 0.135i	-0.038 - 0.227i
Front right wheel vertical motion (z_{u2})	-0.016 - 0.011i	-0.049 - 0.060i	0.109 + 0.110i	1.000 + 0.000i	-1.000 + 0.000i	0.003 + 0.135i	0.038 + 0.227i
Rear left wheel vertical motion (z_{u3})	0.013 + 0.010i	0.106 + 0.190i	0.038 + 0.031i	-0.011 - 0.134i	0.040 + 0.226i	1	1.000 - 0.000i
Rear right wheel vertical motion (z_{u4})	-0.013 - 0.010i	0.106 + 0.190i	0.038 + 0.031i	-0.011 - 0.134i	-0.040 - 0.226i	1.000 + 0.000i	-1.000 + 0.000i
A vehicle with additional HIS system	**Roll**	**Pitch**	**Bounce**	**Front wheel synchronized**	**Front wheel asynchronized**	**Rear wheel synchronized**	**Rear wheel asynchronized**
Eigenvalue (λ_n)	-1.5776±11.1740i	-4.6603±7.7610i	-2.4984±7.1515i	-45.7087±57.1952i	-10.9879±71.1137i	-45.5222±56.4701i	-6.1829±69.5096i
Damped natural frequency (Hz) and damping ratio	f_n=1.778; ζ_n=0.140;	f_n=1.235; ζ_n=0.515;	f_n=1.138; ζ_n=0.330;	f_n=9.103; ζ_n=0.624;	f_n=11.318; ζ_n=0.153;	f_n=8.988; ζ_n=0.628;	f_n=11.063; ζ_n=0.089;
Sprung mass vertical motion (z_s)	0.000 + 0.000i	0.483 - 0.003i	1	-0.056 - 0.050i	0.000 - 0.000i	-0.013 - 0.063i	0.000 + 0.000i
Sprung mass roll motion (ϕ)	1	-0.000 + 0.000i	-0.000 - 0.000i	-0.000 - 0.000i	-0.050 - 0.069i	0.000 + 0.000i	0.013 - 0.010i
Sprung mass pitch motion (θ)	0.000 + 0.000i	1	-0.341 + 0.003i	0.008 + 0.052i	0.000 + 0.000i	-0.052 - 0.065i	-0.000 - 0.000i
Front left wheel vertical motion (z_{u1})	0.060 + 0.023i	-0.015 - 0.076i	0.101 + 0.139i	1.000 - 0.000i	1	-0.081 + 0.274i	-0.835 + 0.340i
Front right wheel vertical motion (z_{u2})	-0.060 - 0.023i	-0.015 - 0.076i	0.101 + 0.139i	1	-1.000 - 0.000i	-0.081 + 0.274i	0.835 - 0.340i
Rear left wheel vertical motion (z_{u3})	0.057 + 0.021i	0.050 + 0.236i	0.029 + 0.040i	0.063 - 0.280i	0.833 - 0.349i	1.000 + 0.000i	1
Rear right wheel vertical motion (z_{u4})	-0.057 - 0.021i	0.050 + 0.236i	0.029 + 0.040i	0.063 - 0.280i	-0.833 + 0.349i	1.000 + 0.000i	-1.000 + 0.000i

dividing the corresponding maximum value, max(abs($\boldsymbol{X}$)). The normalized mode shapes can be used to identify the vehicle modes, such as vertical, roll, pitch, etc, as shown in Tab.1.

As shown in Fig.1, the original suspension system consists of spring and damper parts, in which the modal parameters of vehicle vibration modes can be obtained, as shown in Tab.1. Because the accumulators and damper valves can affect the stiffness and damping, the vibration mode shapes and frequencies are changed correspondingly after the HIS system is installed, which is shown in Tab.1. Tab.1 indicates that the HIS system can significantly enhance vibration stiffness for roll mode without touching other modes. The vibration modes can be decoupled by HIS system with special connection configuration of hydraulic chambers.

B. HIS SYSTEM MODEL

The cylinder connections of HIS system in the roll plane is shown in Fig.3. HIS system consists of four cylinders in four suspension stations, oil pipelines, two accumulators and four damping valves. During certain maneuvers, such as steering, in one circuit, vehicle body rolls around its longitudinal axis, the suspension is contracted and the oil in cylinder chambers is pushed to the accumulator in Circuit A. Then the air volume in accumulator decreases and oil pressure rises. The same is for the other circuit. The pressure differences in upper

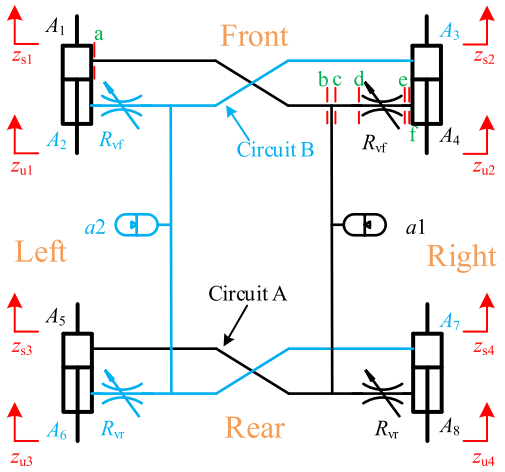

FIGURE 3. The schematic diagram of the HIS system.

and lower chambers of cylinders generate an opposite roll moment, which pushes the vehicle body back to the normal status.

In HIS system, the upper chambers of cylinders are connected with the vehicle body, and lower chamber is connected with unsprung mass, as shown in Fig.3. The displacements at the upper end of the suspension z_{si} (i = 1,2,3,4) are the same as the connection points on the vehicle body. The upper displacements are written into a vector form $\boldsymbol{Z}_s = [z_{s1}, z_{s2}, z_{s3}, z_{s4};]^T$. Knowing the geometry, it can also be rewritten as:

$$\boldsymbol{T}_z = \begin{bmatrix} 1 & t_f & -l_f \\ 1 & -t_f & -l_f \\ 1 & t_r & l_r \\ 1 & -t_r & l_r \end{bmatrix} \tag{6}$$

Then the change of the chamber volume in upper chambers ΔV_{Hti} and lower chambers ΔV_{Hbi} can be obtained:

$$\begin{aligned} \Delta V_{Hti} &= A_{ti}\,(z_{si} - z_{ui}) \\ \Delta V_{Hbi} &= -A_{bi}\,(z_{si} - z_{ui}) \end{aligned} \tag{7}$$

where the areas of upper chambers A_{ti} and lower chambers A_{bi} can be obtained with the inner diameters of cylinders (d_{fi}, d_{ri}) and outer diameters of corresponding pistons (d_{fo}, d_{ro}), where subscripts 'f' and 'r' denote front and rear axles, respectively, and subscripts 'i' and 'o' denotes inner and outer diameters, respectively.

Using Circuit A as an example, state variables in one chamber are affected by other chambers. The transformation matrix can be used to describe this relationship:

$$\begin{bmatrix} p_{2b}\,(s) \\ q_{2b}\,(s) \end{bmatrix} = \boldsymbol{T}^A_{2\leftarrow 1} \begin{bmatrix} p_{1t}\,(s) \\ q_{1t}\,(s) \end{bmatrix} \tag{8}$$

where $\boldsymbol{T}^A_{2\leftarrow 1} = \boldsymbol{T}_{fe}\boldsymbol{T}_{ed}\boldsymbol{T}_{dc}\boldsymbol{T}_{cb}\boldsymbol{T}_{ba}$ is the state transformation matrix between the front-left upper chamber and the front-right lower chamber, which is a 2 by 2 matrix:

$$\boldsymbol{T}^A_{2\leftarrow 1} = \begin{bmatrix} T_{11} & T_{12} \\ T_{21} & T_{22} \end{bmatrix} \tag{9}$$

The elements in $\boldsymbol{T}^A_{2\leftarrow 1}$ are nonlinear functions of the hydraulic systems. For example, $T_{11} = f(V_{A0}, p_{A0}, R_{vf}, R_{vr}, d_p, t_p, \rho, \gamma)$, in which V_{A0}, p_{A0} are the pre-charged initial air volume and initial oil pressure of accumulator in Circuit A, respectively. Generally, the oil pressure loss at the damper valves can be expressed as:

$$\Delta p_i = R_{vi}Q_{vi} = R_{vi}A_{bi}\,(\dot{z}_{si} - \dot{z}_{ui}) \tag{10}$$

Then the Eq.(8) and Eq.(9) are integrated, as follows:

$$\begin{bmatrix} p_{1t}\,(s) \\ p_{2b}\,(s) \end{bmatrix} = \begin{bmatrix} -\dfrac{T_{22}}{T_{21}} & \dfrac{1}{T_{21}} \\ T_{12} - \dfrac{T_{11}}{T_{21}}T_{22} & \dfrac{T_{11}}{T_{21}} \end{bmatrix} \begin{bmatrix} q_{1t}\,(s) \\ q_{2b}\,(s) \end{bmatrix} \tag{11}$$

Similarly, the relationships between the state variables in the left-front upper chamber, the left-rear upper chamber and right-rear lower chamber can also be obtained. The oil pressures can be determined by oil flow quantities in Circuit A. Eq.(11) can be written as a compact form:

$$\boldsymbol{P}_A\,(s) = \boldsymbol{T}^A_{\boldsymbol{P}\leftarrow\boldsymbol{Q}}\boldsymbol{Q}_A\,(s) \tag{12}$$

where $\boldsymbol{P}_A$ and $\boldsymbol{Q}_A$ are oil pressure states and flow quantity states in Circuit A, respectively. $\boldsymbol{T}^A_{P\leftarrow Q}$ is the corresponding state transformation matrix.

Similarly, the states transmitting in Circuit B can be written as:

$$\boldsymbol{P}_B\,(s) = \boldsymbol{T}^B_{\boldsymbol{P}\leftarrow\boldsymbol{Q}}\boldsymbol{Q}_B\,(s) \tag{13}$$

Then combining Eq.(12) and Eq.(13), the state variables of the entire system can be obtained:

$$\boldsymbol{P}\,(s) = \boldsymbol{T}_{\boldsymbol{P}\leftarrow\boldsymbol{Q}}\boldsymbol{Q}\,(s) \tag{14}$$

where $\boldsymbol{P}\,(s) = \left[\boldsymbol{P_A}\,(s)\ \boldsymbol{P_B}\,(s)\right]^T$, $\boldsymbol{Q}\,(s) = \left[\boldsymbol{Q_A}\,(s)\ \boldsymbol{Q_B}\,(s)\right]^T$, $\boldsymbol{T}_{\boldsymbol{P}\leftarrow\boldsymbol{Q}} = \begin{bmatrix} \boldsymbol{T}^A_{\boldsymbol{P}\leftarrow\boldsymbol{Q}} & 0 \\ 0 & \boldsymbol{T}^B_{\boldsymbol{P}\leftarrow\boldsymbol{Q}} \end{bmatrix}$.

For Circuit A, flow quantities in cylinders are determined by the suspension contraction:

$$\boldsymbol{Q}_A\,(s) = s\left[A_{1t}\ -A_{2b}\ A_{3u}\ -A_{4b}\right]\left[\boldsymbol{Z}_s - \boldsymbol{Z}_u\,(s)\right] \tag{15}$$

where $\boldsymbol{Z}_u(t) = [z_{u1}, z_{u2}, z_{u3}, z_{u4};]^T$.

Eq.(15) can be rewritten as:

$$\boldsymbol{Q}_A\,(s) = s\boldsymbol{T}^A_{\boldsymbol{Q}\leftarrow\boldsymbol{X}}\boldsymbol{X}\,(s) \tag{16}$$

where $\boldsymbol{T}^A_{\boldsymbol{Q}\leftarrow\boldsymbol{X}} = \left[A_{1t}\ -A_{2b}\ A_{3u}\ -A_{4b}\right]\left[\boldsymbol{T}_z\ -\boldsymbol{I}_{(4\times 4)}\right]$.

The same is done for Circuit B, the flow quantities in the entire HIS system in terms of the vehicle state variables can be obtained:

$$\boldsymbol{Q}\,(s) = s\boldsymbol{T}_{\boldsymbol{Q}\leftarrow\boldsymbol{X}}\boldsymbol{X}\,(s) \tag{17}$$

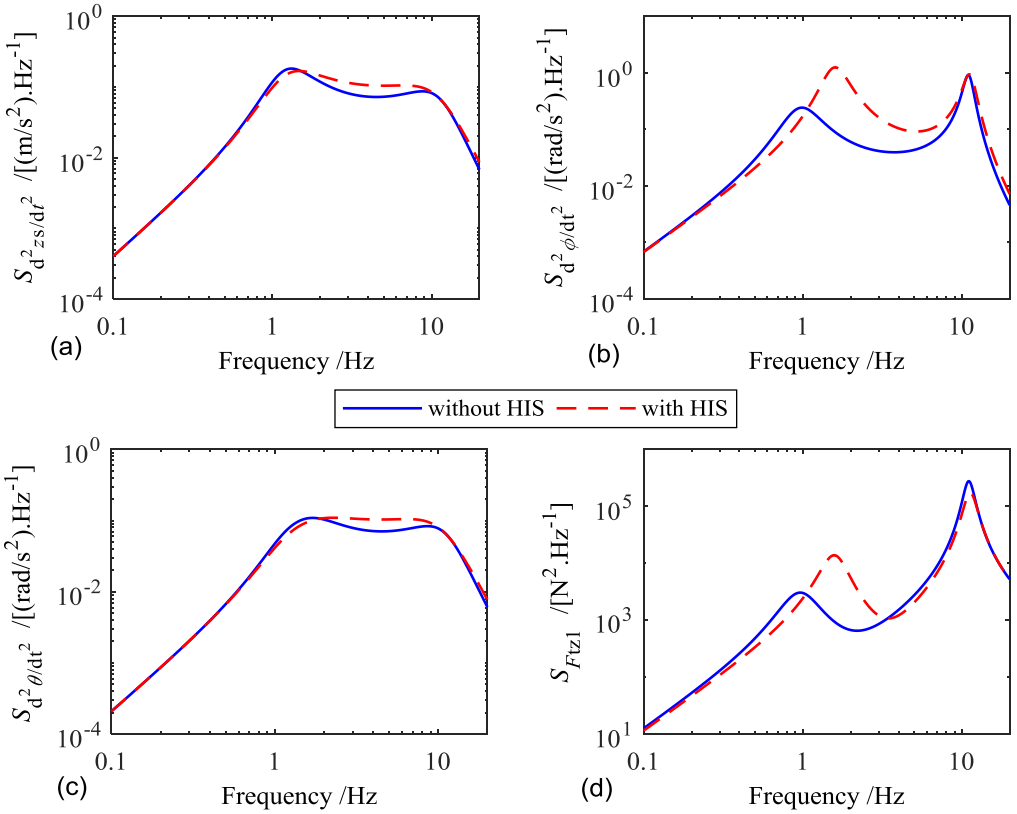

FIGURE 4. Comparison of the response spectrum between the vehicle with HIS and vehicle without HIS (a) vertical acceleration at CG; (b) roll angular acceleration; (c) pitch angular acceleration; (d) vertical tire ground force at the left-front wheel at roll motion.

Also, generated by the HIS system, the forces applying on the vehicle body can be written as:

$$\boldsymbol{F}_{\mathrm{Hs}}(s) = \boldsymbol{T}_{\boldsymbol{F}\leftarrow\boldsymbol{P}}\boldsymbol{P}(s) \tag{18}$$

where $P(t) = \left[p_{1t}\ p_{1b}\ p_{2t}\ p_{2b}\ p_{3t}\ p_{3b}\ p_{4t}\ p_{4b}\right]^T$, $\boldsymbol{T}_{F\leftarrow P}$ is the state transformation matrix between the oil pressures and the forces that are generated.

$$\boldsymbol{T}_{\boldsymbol{F}\leftarrow\boldsymbol{P}} = \begin{bmatrix} A_{1t} & -A_{1b} & 0 & 0 & 0 & 0 & 0 & 0 \\ 0 & 0 & A_{2t} & -A_{2b} & 0 & 0 & 0 & 0 \\ 0 & 0 & 0 & 0 & A_{3t} & -A_{3b} & 0 & 0 \\ 0 & 0 & 0 & 0 & 0 & 0 & A_{4t} & -A_{4b} \end{bmatrix}.$$

Eq.(18) can be rewritten as:

$$\boldsymbol{F}_{\mathrm{H}}(s) = \begin{bmatrix} \boldsymbol{T}_z^T \\ -\boldsymbol{I}_{(4\times4)} \end{bmatrix} \boldsymbol{T}_{\boldsymbol{F}\leftarrow\boldsymbol{P}}\boldsymbol{P}(s) \tag{19}$$

C. VEHICLE MODEL COUPLED WITH HIS SYSTEM

The Laplace transformation is performed on both Eq.(2) and Eq.(19), the dynamic equation of the coupled system can be written as:

$$s^2\boldsymbol{M}\boldsymbol{X}(s) + s\boldsymbol{C}\boldsymbol{X}(s) + \boldsymbol{K}\boldsymbol{X}(s) = \boldsymbol{F}(s) + \boldsymbol{F}_{\mathrm{H}}(s) \tag{20}$$

Based on Eq.(14), (17) and (19), transformation matrix between the road disturbance $\boldsymbol{Z}_{\mathrm{g}}(s)$ and the vehicle state variables $\boldsymbol{X}(s)$ can be obtained:

$$\boldsymbol{H}(s) = \left[s^2\boldsymbol{M} + s\left(\boldsymbol{C} - \begin{bmatrix} \boldsymbol{T}_z^T \\ -\boldsymbol{I}_{4\times4} \end{bmatrix}\boldsymbol{T}_{\boldsymbol{F}\leftarrow\boldsymbol{P}}\boldsymbol{T}_{\boldsymbol{P}\leftarrow\boldsymbol{Q}}\boldsymbol{T}_{\boldsymbol{Q}\leftarrow\boldsymbol{X}}\right) + \boldsymbol{K}\right]^{-1}\boldsymbol{T}_{\boldsymbol{F}\leftarrow\boldsymbol{Z}} \tag{21}$$

Then the transformation matrix between the road disturbances and the states accelerations can be obtained:

$$\boldsymbol{H}_{\ddot{\boldsymbol{X}}}(s) = s^2\boldsymbol{H}(s) \tag{22}$$

And, transformation matrix between the road disturbances and the tire ground forces can be written as:

$$\boldsymbol{H}_{\boldsymbol{F}}(s) = \boldsymbol{K}_{\mathrm{t}}\left(\boldsymbol{H}_{\boldsymbol{Z}_{\mathrm{u}}}(s) - \boldsymbol{I}_{4\times4}\right) \tag{23}$$

where $\boldsymbol{H}_{\boldsymbol{Z}_u}(s)$ is the bottom four rows in $\boldsymbol{H}(s)$.

Then the power spectrum density (PSD) for a generalized transfer function $\boldsymbol{H}(s)$ can be obtained:

$$\boldsymbol{S}_{\boldsymbol{H}} = \boldsymbol{H}^*\boldsymbol{S}_{z_g}\boldsymbol{H} \tag{24}$$

where $\boldsymbol{S}_{zg}$ is the PSD matrix for road disturbance inputs; and superscript $*$ denotes the conjugate transposition of the matrix.

Compared with the function in the frequency domain in reference [5], [37] which often has more than 10 DOFs due

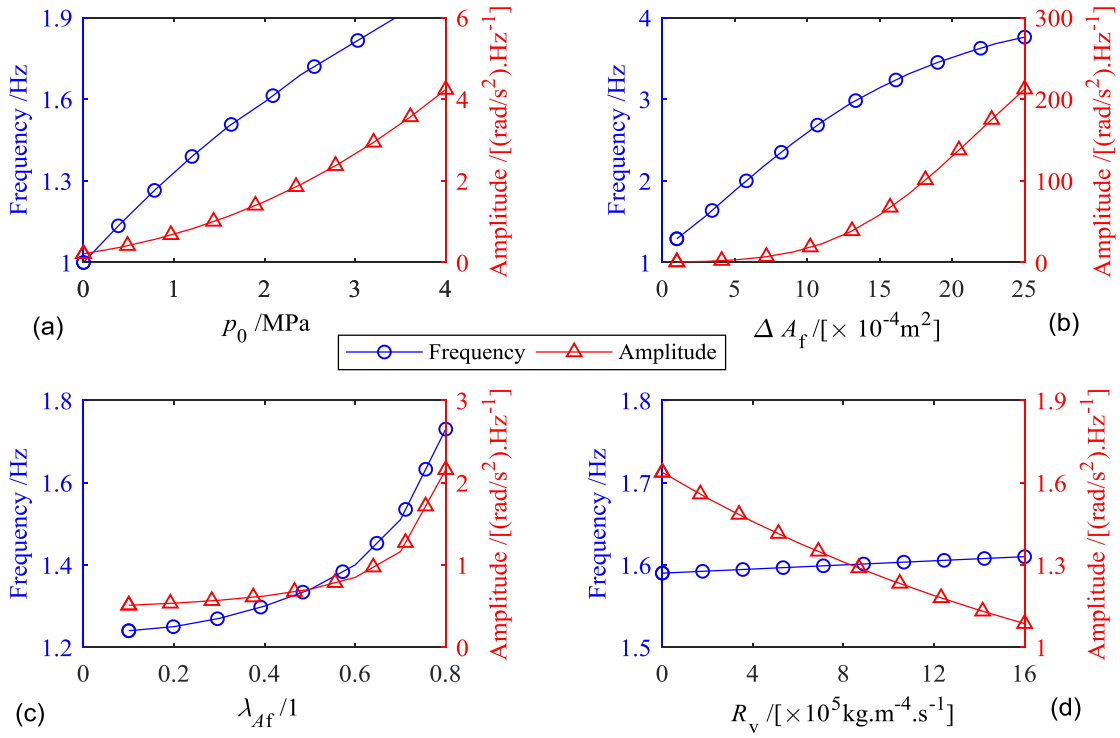

FIGURE 5. The effects of the HIS parameters variations on the roll mode of the vehicle (a) pre-charged initial oil pressure p_0; (b) area difference between the upper and lower chamber ΔA_f; (c) area ratio between the upper and lower chamber λ_{Af}; (d) damper valves coefficient R_v.

to the DOFs of the HIS system, the proposed model shown in Eq.(20) only has 7 state variables. This increases the computational speed and facilitates the analysis process.

III. COMPARISON OF THE RESPONSE BETWEEN THE VEHICLE WITH HIS AND THE REFERENCE VEHICLE

The vertical acceleration, roll acceleration, pitch acceleration and tire ground forces are selected as indicators to assess the vehicle dynamic behavior, specifically, the ride performance. Instead of using the Root Mean Square (RMS) of the responses in the time domain, the responses frequency spectrum is evaluated. Based on the standard, ISO 2631.1 (ISO 2631,1997), the road inputs of class C with road spectrum density $S_q(n_0) = 256\times10^{-6}\text{m}^3$ under reference spatial frequency $n_0 = 0.1\text{m}^{-1}$ is used for the simulation. The nonlinear terms, like $p = p_0\left(V_0/(V_0-\Delta V)\right)^{\gamma}$ shown in Eq.(19), are linearized to its equilibrium position (the status when the HIS system is pre-charged to its initial condition) as $p = p_0\left(1+\gamma\Delta V/V_0\right)$. The simulation is performed at a vehicle speed of $v = 10$ m/s. The responses spectrum of the four indicators is shown in Fig.4. The vehicle with the HIS system and the reference vehicle are compared.

IV. EFFECTS OF THE HIS PARAMETERS VARIATIONS ON THE VEHICLE DYNAMICS

The effects of HIS physical parameter variations on the vehicle dynamic characteristics are studied. Four physical parameters of the HIS system are used as independent variables:

TABLE 2. The value range of the physical parameters in the HIS system.

Parameters	Lower Bound	Upper Bound
p_0 /MPa	0.0	4.0
ΔA_f /×10⁻⁴ m²	1.0	25.0
λ_{Af} /1	0.1	0.8
R_v /×10⁵ kg·m⁻⁴·s⁻¹	0.0	16.0

(a) pre-charged initial oil pressure p_0;
(b) area difference between the upper and lower chamber ΔA_f;
(c) area ratio between the upper and lower chamber λ_{Af};
(d) damper valves coefficient R_v.

Due to the similarity of the vehicle dynamic behavior between the front and rear half vehicle, only the front axle is studied. The variation range of the physical parameters in the HIS system is shown in Tab.2.

The effects of HIS physical parameter variations on four vehicle modes are investigated in Section IV. They are roll mode, pitch mode, bounce mode, and tire ground force. Two indicators, first-order frequency of each mode and the maximum amplitude of each modal response, are used to characterize the static and dynamic behavior of each vehicle mode. The effects of the four HIS parameters variations on these two indicators are investigated, respectively.

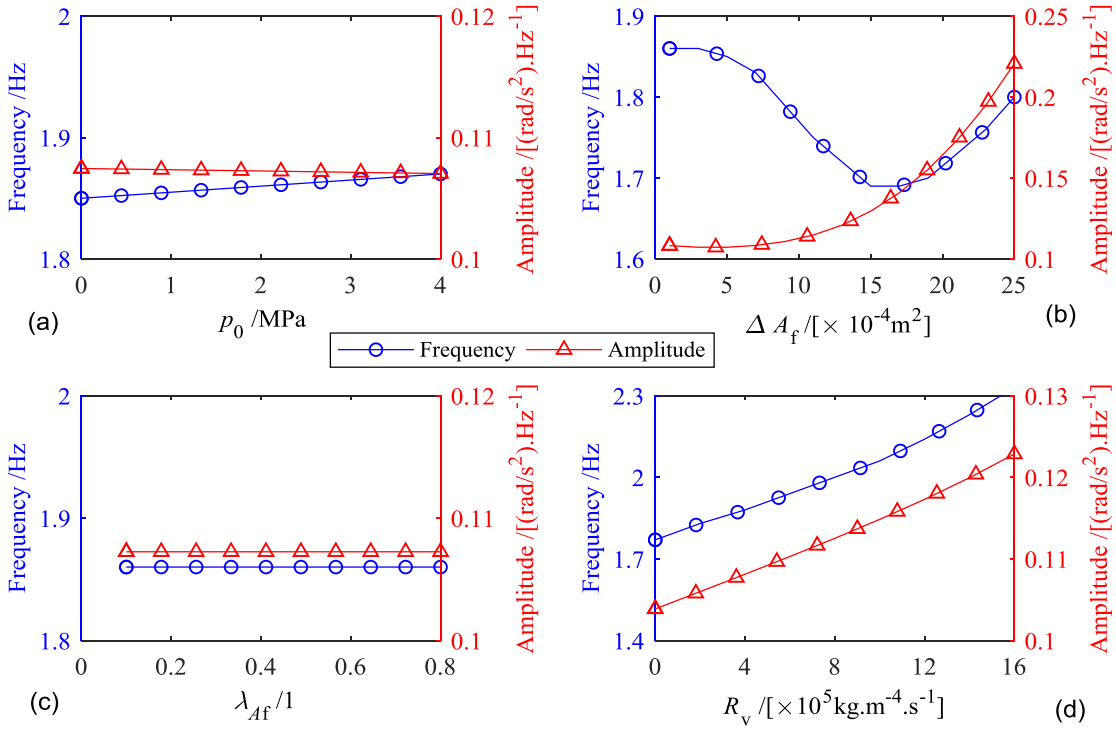

FIGURE 6. The effects of the HIS parameters variations on the pitch mode of the vehicle (a) pre-charged initial oil pressure p_0; (b) area difference between the upper and lower chamber ΔA_f; (c) area ratio between the upper and lower chamber λ_{Af}; (d) damper valves coefficient R_v.

A. EFFECTS ON ROLL MODE

In Fig.5 (a), as the pre-charged oil pressure p_0 increases, the frequency of the roll mode goes higher, and the roll mode becomes stiffer. Higher response amplitude indicates more energy consumed. In Fig.5 (b) and (c), both frequency and maximum response amplitude increase with an increase of either the area difference ΔA_f or area ratio λ_{Af} between the upper and lower chamber. In Fig.5 (d), an increase in the damper valves coefficient R_v produces a decrease in the response amplitude and a slight increase in the frequency. Among the four parameters, the roll mode is most sensitive to the area difference ΔA_f.

B. EFFECTS ON PITCH MODE

The same is done for the pitch mode, as shown in Fig.6. In Fig.6 (a) and (c), as the pre-charged oil pressure p_0 or area ratio λ_{Af} increase, both frequency, and maximum response amplitude remain constant. In Fig.6 (b), the maximum response amplitude increases with increasing area difference ΔA_f, whereas, as the area difference ΔA_f increases, the frequency has a decrease until $\Delta A_f = 15\times10^{-4}\text{m}^2$ and increases after that. When the vehicle motion is dominated by the pitch mode, the oil volume transferred from the front cylinders to the accumulators are unchanged. Thus, the pitch stiffness is not affected by these two factors. In Fig.6 (d), an increase in the damper valves coefficient R_v produces an increase in both frequency and response amplitude. Among the four parameters, the pitch mode is most sensitive to the area difference ΔA_f and damper valves coefficient R_v.

C. EFFECTS ON BOUNCE MODE

In Fig.7 (a) and (b), as the pre-charged oil pressure p_0 or area difference ΔA_f increase, both frequency, and maximum response amplitude have an increase. When a vehicle has a bounce motion, the volume of oil pumped into the accumulator's increases as ΔA_f increases. Because the air volume is constant, the vertical compressibility becomes worse, and the vertical frequency increases. In Fig.7 (c), both frequency and maximum response amplitude remain unchanged, which indicates that the bounce mode is independent of the area difference ΔA_f. In Fig.7 (d), the frequency increases with the increasing damper valves coefficient R_v, whereas, R_v doesn't have a great influence on the response amplitude. Thus, area difference ΔA_f is the most sensitive factor for the bounce mode.

D. EFFECTS ON TIRE GROUND HOLDING ABILITY

In Fig.8 (a) and (c), the frequency of the tire ground force increases with the increasing pre-charged oil pressure p_0 and area ratio λ_{Af},whereas, the maximum response amplitude decreases. In Fig.8(b), the frequency of the tire ground force and the maximum response amplitude reach their minimum

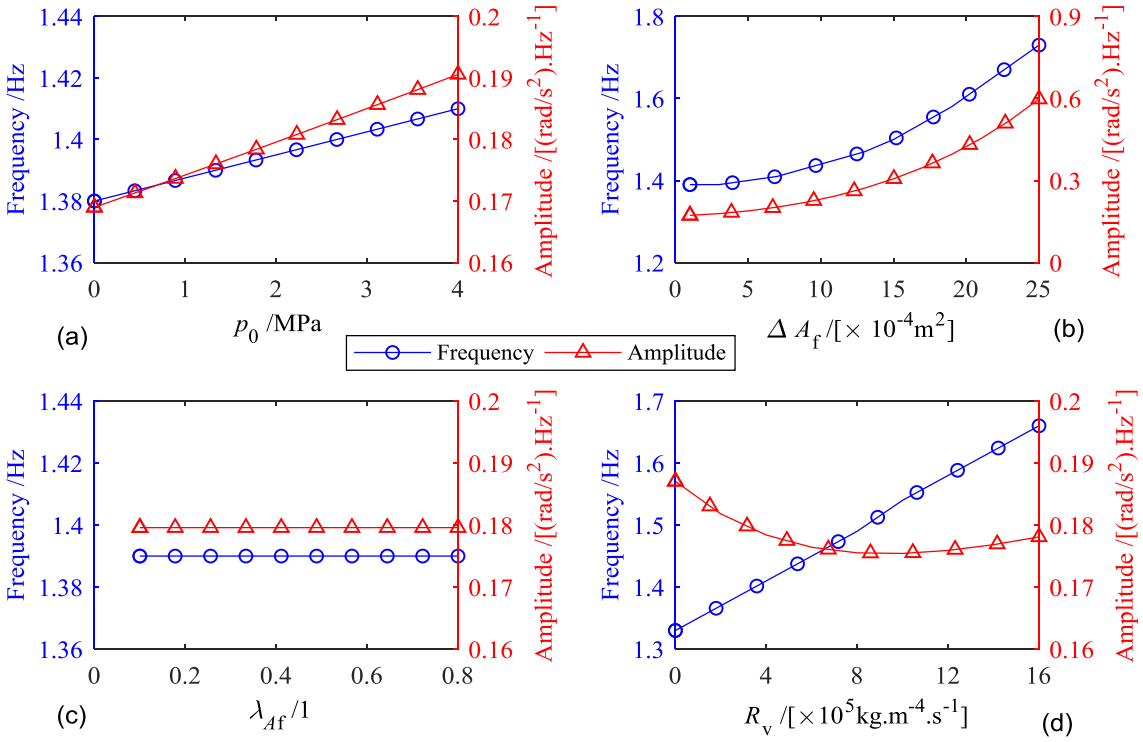

FIGURE 7. The effects of the HIS parameters variations on the vertical acceleration of the vehicle (a) pre-charged initial oil pressure p_0; (b) area difference between the upper and lower chamber ΔA_f; (c) area ratio between the upper and lower chamber λ_{Af}; (d) damper valves coefficient R_v.

when $\Delta A_f = 15\times10^{-4}m^2$. In Fig.8 (d), the damper valves coefficient R_v doesn't have great influence on both frequencies of the tire ground force and its response Amplitude. Overall, pre-charged oil pressure p_0 has the greatest effect on the frequency, while the area difference ΔA_f affects the response amplitude a lot.

V. DESIGN AND OPTIMIZATION OF THE HIS PARAMETERS

The value of the four HIS parameters shown in the previous section are optimized and tuned to make the vehicle having a better ride comfort and handling stability. These four parameters determine the additional compressibility and damping properties of the HIS system. When the area difference of the upper and lower chamber of the cylinder ΔA_f and the area ratio λ_{Af} are studied, the pre-charged oil pressure p_0 and damper valves coefficient R_v remain constant, and vice versa.

The four indicators for evaluating the vehicle ride comfort and handling stability are as follows:

(1) Total frequency-weighted acceleration RMS value σ_{aw};
(2) The maximum vehicle roll angle max(S_ϕ);
(3) The maximum suspension stroke max(S_{zsu1});
(4) The dynamic tire load max(S_{Ftz1}).

For roll-resistant HIS system, the physical parameters are designed to obtain small roll angle. Also, the stroke of the suspension also needs to be designed to avoid interference of the sprung and unsprung mass. Also, the dynamic tire load should also meet the requirement for handling stability. The total frequency-weighted acceleration RMS value σ_{aw} is derived as follows.

Based on ISO 2631 standard, the RMS values σ can be derived from Eq.(25):

$$\sigma^2 = \sum_{\omega_l \le \omega \le \omega_u} \boldsymbol{S_H} \Delta\omega \tag{25}$$

where ω_l and ω_u denote the lower and upper bound of the circular frequencies, respectively; $\Delta\omega$ is the circular frequency interval. The RMS values for bounce, roll and pitch modes can be calculated using Eq.(25) in each one-third octave frequency band with a frequency range from 0.5 Hz to 80 Hz. The frequency weighted RMS values can be obtained by multiplying the RMS values with frequency weighting coefficients w_{ji} ($j = x, y, z$). The total frequency weighted RMS values σ_{aw} is determined by the axis weighting factors k_i ($i = x, y, z$):

$$\sigma_{aw}^2 = k_x \sum_{\omega_l \le \omega \le \omega_u} w_{xi}^2 \sigma_{axi}^2 + k_y \sum_{\omega_l \le \omega \le \omega_u} w_{yi}^2 \sigma_{ayi}^2 + k_z \sum_{\omega_l \le \omega \le \omega_u} w_{zi}^2 \sigma_{azi}^2 \tag{26}$$

where a_x, a_y is the longitudinal and translational acceleration of vehicle body, respectively, $a_x = h_{os}\ddot{\theta}$, $a_y = -h_{os}\ddot{\phi}$.

Fig.9 shows that smaller λ_{Af} and ΔA_f can result in better performance in the feasible region in max(S_ϕ)-σ_{aw}^2

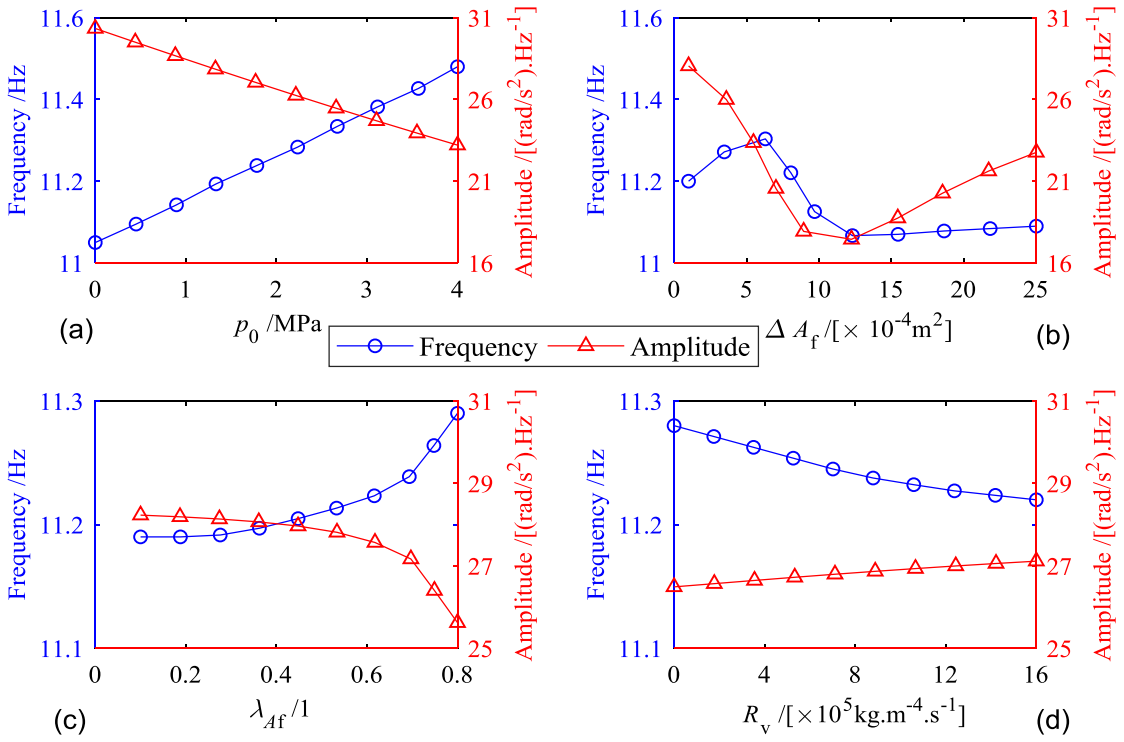

FIGURE 8. The effects of the HIS parameters variations on the tire ground force at the left-front wheel (a) pre-charged initial oil pressure p_0; (b) area difference between the upper and lower chamber ΔA_f; (c) area ratio between the upper and lower chamber λ_{Af}; (d) damper valves coefficient R_v.

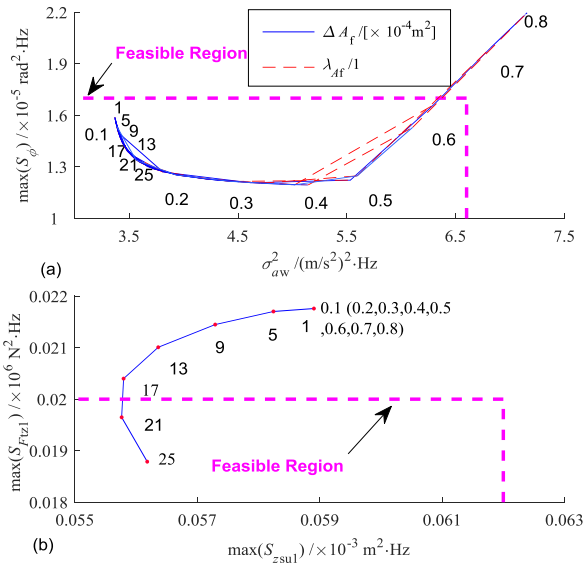

FIGURE 9. Tuning of both area difference of the upper and lower chamber of the cylinder ΔA_f and the area ratio λ_{Af}. (a) Total frequency-weighted RMS value of accelerations in CG and maximum vehicle roll angle. (b) Maximum suspension stroke and dynamic tire load at the left-front wheel.

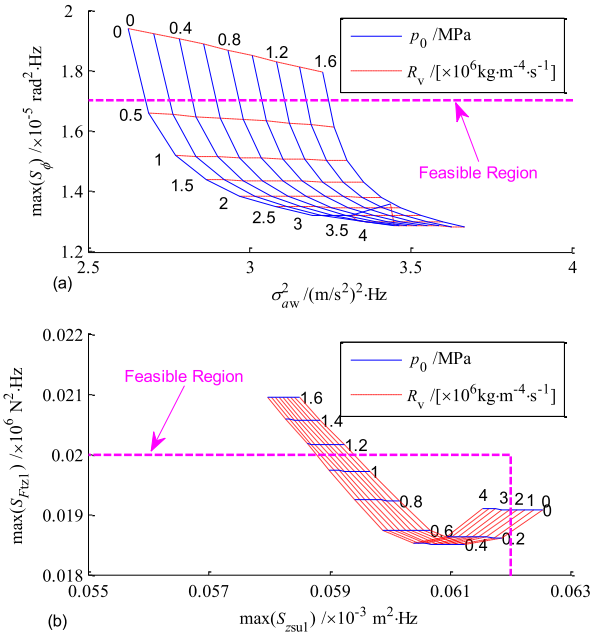

FIGURE 10. Tuning of both pre-charged initial oil pressure p_0 and damper valves coefficient R_v. (a) Total frequency-weighted RMS value of accelerations in CG and maximum vehicle roll angle. (b) Maximum suspension stroke and dynamic tire load at the left-front wheel.

coordinate system. The λ_{Af} value has no effect on the indicators of $\max(S_{zsu1})$ and $\max(S_{Ftz1})$.The increase of ΔA_f will significantly decrease both $\max(S_{zsu1})$ and $\max(S_{Ftz1})$, the larger ΔA_f can minimize the dynamic tire load $\max(S_{Ftz1})$. As shown in Fig.10, in $\max(S_\phi)$-σ^2_{aw} coordinate system, we can't minimize $\max(S_\phi)$ and σ_{aw}, simultaneously, it requires p_0 is larger than 0.4 MPa. The $\max(S_\phi)$ value

FIGURE 11. Full vehicle drop test (a) test set up; (b) front axle drop test; (c) right side drop test; (d) all wheels drop test.

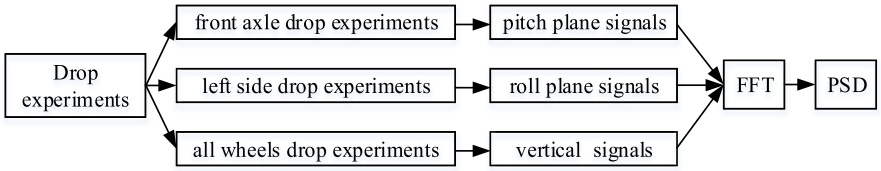

FIGURE 12. Flow chart of the test procedure.

decreases when p_0 increases, and the σ_{aw} will increase, which still is within the feasible domain. In $\max(S_{Ftz1})$-$\max(S_{zsu1})$ coordinate system, R_V has a greater impact on both indicators than p_0, it requires that p_0 should be as much larger as possible when R_V is smaller than 1.2×10^6 kg·m^{-4}·s^{-1}, and the minima of $\max(S_{Ftz1})$ can be reached when $R_V = 1.2\times10^6$kg·m^{-4}·s^{-1}.

There is a trade off between the physical parameters of HIS. The physical parameters of HIS need to be coordinately tuned instead of being independently designed. The feasible regions for the four physical parameters can be obtained with the requirement for the indicators are known, as shown by the dash lines in figures.

VI. EXPERIMENTAL VALIDATION

To validate the proposed condensed frequency-domain vehicle model, the full vehicle drop test is performed to compare the experimental results with the analytical results. The vehicle vibration usually combines a couple of modes. A set of full vehicle drop tests is performed, and the aim is to excite the vertical, roll and pitch mode separately. In this way, the overall vibration is dominated by one mode, which makes it easier to extract the mode shape and frequency of this dominant mode. The test set up is shown in Fig.11. Three sets of tests are performed, front axle drop test, left side drop test and all wheels drop test, with pitch mode, roll mode and bounce mode mainly be excited, respectively. The test procedure is shown in Fig.12.

In the analytical study, the effects of the variation of four parameters of HIS system on the vehicle dynamic behavior is studied. In the test, only the pre-charged oil pressure p_0 is selected as a variable for the experimental validation, due to its easy implementation. In the test, three different oil pressure p_0 is adopted, 1.0 MPa, 2.0 MPa, and 3.0 MPa. Eight well-calibrated accelerators are instrumented on the sprung and unsprung mass. The time signal is collected using the data acquisition system [38], [39], and then processed using a low-pass filter with a 20.0 Hz cut-off frequency. The measured response spectrum of the three modes, roll, pitch, and bounce are shown in Fig.13 (a), (c) and (d), respectively, along with analytical response spectrum of the roll mode shown in Fig.13 (b). The extracted measured frequencies are shown and compared with the analytical frequencies in Tab.3.

In Fig.13 (a) and (b), the analytical response spectrum of the roll mode has a good agreement with the measured data. As shown inTab.3, of each mode, the analytical frequencies

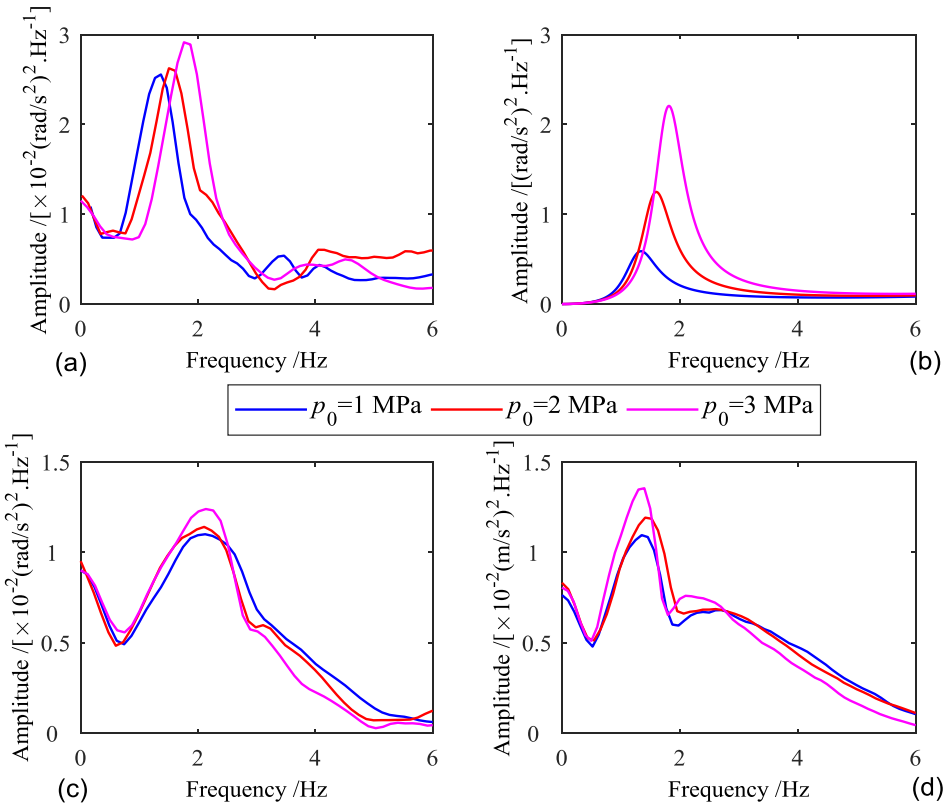

FIGURE 13. The response spectrum of the vehicle modes with different pre-charged oil pressure p0 (a) roll mode (measured); (b) roll mode (analytical); (c) pitch mode (measured); (d) bounce mode (measured).

TABLE 3. Comparison of measured frequencies of vehicle modes with analytical frequencies/Hz.

	p_0= 1.0 MPa			p_0= 2.0 MPa			p_0= 3.0 MPa		
	*S	*E	error /%	*S	*E	error /%	*S	*E	error /%
*Roll	1.342	1.367	1.86	1.600	1.504	-6.00	1.816	1.760	-3.08
*Pitch	2.279	2.122	-6.89	2.285	2.105	-7.88	2.291	2.133	-6.90
*Bounce	1.467	1.353	-7.78	1.471	1.413	-3.94	1.476	1.398	-5.28

*Note: *S denotes 'Simulation'; *E denotes 'Experiment'

are quite close to the extracted measured frequencies with the error of less than 10%. This good comparison could greatly validate the effectiveness of the proposed vehicle model.

In Tab.3, among the three vehicle modes, only the roll mode would become stiffer with an increase of the oil pressure. Also, no matter the oil pressure, the frequencies of the roll mode are very close to the bounce mode. There are errors between measured and analytical frequencies. The reasons are as follows: 1) the actual initial oil pressure p_0 and accumulator volume V_0 usually has a slight error with the parameters used in the simulation. 2) vehicle parameters identified from the parameter estimation might have errors [21]. However, overall, a very good comparison between measured and analytical data has been obtained.

VII. CONCLUSION

New frequency-based modeling for a vehicle with HIS system has been developed. The proposed vehicle model has much fewer DOFs than the conventional modeling approach. The advantage of the HIS system over the reference vehicle is stated via analytical comparison. The effects of the HIS system parameters on the several vehicle modes indicators are analytically investigated, which could provide a guideline for the parameter tuning of the parameters. The HIS system parameters are also coordinately optimized to meet the ride comfort requirement. The full vehicle lab tests are conducted to validate the proposed vehicle model. A very good comparison has been obtained between the analytical and experimental results. The validated proposed vehicle

TABLE 4. Vehicle parameters.

Name	Value	Description
m_s /kg	1370	Vehicle sprung mass
m_{uf} /kg	42	Vehicle unsprung mass of each suspension in the front axle
m_{ur} /kg	42	Vehicle unsprung mass of each suspension in the rear axle
I_{xx} /kg·m^2	291	Sprung mass moment of inertia about the x-axis (about CG)
I_{yy} /kg·m^2	1973	Sprung mass moment of inertia about the y-axis (about CG)
c_{sf} /N·s·m^{-1}	2600	Spring damping at each suspension station in the front axle
c_{sr} /N·s·m^{-1}	2300	Spring damping at each suspension station in the rear axle
k_{sf} /N·m^{-1}	24000	Spring stiffness at each suspension station in the front axle
k_{sr} /N·m^{-1}	20000	Spring stiffness at each suspension station in the rear axle
k_{tf} /N·m^{-1}	200000	Tire stiffness at the front wheel
k_{tr} /N·m^{-1}	200000	Tire stiffness at the rear wheel
l_f /m	1.11	Distance from the sprung mass CG to the front axle
l_r /m	1.67	Distance from the sprung mass CG to the rear axle
t_f /m	0.77	The half width of front wheels
t_r /m	0.77	The half width of rear wheels

TABLE 5. Physical parameters of the HIS system.

Name	Value	Description
p_0 /MPa	2.0	Initial oil pressure pre-charged in the HIS system
V_0 /L	0.54	The initial air volume of accumulators when the pre-charging process is completed
R_{vf} /kg·s^{-1}·m^{-4}	6×10^5	Pressure loss coefficient in front cylinders lower outlets
R_{vr} /kg·s^{-1}·m^{-4}	6×10^5	Pressure loss coefficient in rear cylinders lower outlets
d_{ci} /mm	40	The inner diameter of front/rear axle cylinders
d_{po} /mm	20	The outer diameter of front/rear axle pistons
ΔA_f /m^2	0.0012	Area difference between upper and lower chambers in front cylinders
ΔA_r /m^2	0.0012	Area difference of upper and lower chambers in rear cylinders
λ_{Af} /1	0.75	The area ratio of lower and upper chambers in front cylinders
λ_{Ar} /1	0.75	The area ratio of lower and upper chambers in rear cylinders

model is a great tool for design, parameter tuning, optimization, dynamics study of the vehicle fitted with HIS.

APPENDIX

See Tables 4 and 5.

REFERENCES

[1] W. Sun, Z. Zhao, and H. Gao, "Saturated adaptive robust control for active suspension systems," *IEEE Trans. Ind. Electron.*, vol. 60, no. 9, pp. 3889–3896, Sep. 2013.
[2] H. Li, H. Liu, H. Gao, and P. Shi, "Reliable fuzzy control for active suspension systems with actuator delay and fault," *IEEE Trans. Fuzzy Syst.*, vol. 20, no. 2, pp. 342–357, Apr. 2012.
[3] W. Sun, Y. Zhao, J. Li, L. Zhang, and H. Gao, "Active suspension control with frequency band constraints and actuator input delay," *IEEE Trans. Ind. Electron.*, vol. 59, no. 1, pp. 530–537, Jan. 2012.
[4] Y. Chen, D. Joffre, and P. Avitabile, "Underwater dynamic response at limited points expanded to full-field strain response," *J. Vib. Acoust.*, vol. 140, no. 5, 2018, Art. no. 051016.
[5] N. Zhang, W. A. Smith, and J. Jeyakumaran, "Hydraulically interconnected vehicle suspension: Background and modelling," *Vehicle Syst. Dyn.*, vol. 48, no. 1, pp. 17–40, Jan. 2010.
[6] W. A. Smith, N. Zhang, and J. Jeyakumaran, "Hydraulically interconnected vehicle suspension: Theoretical and experimental ride analysis," *Vehicle Syst. Dyn.*, vol. 48, no. 1, pp. 41–64, 2010.
[7] S. Zhu, H. Du, and N. Zhang, "Development and implementation of fuzzy, fuzzy PID and LQR controllers for an roll-plane active Hydraulically Interconnected Suspension," in *Proc. IEEE Int. Conf. Fuzzy Syst.*, Jul. 2014, pp. 2017–2024.

[8] H. Du and N. Zhang, "Fuzzy control for nonlinear uncertain electrohydraulic active suspensions with input constraint," *IEEE Trans. Fuzzy Syst.*, vol. 17, no. 2, pp. 343–356, Apr. 2009.

[9] D. Cao, S. Rakheja, and C.-Y. Su, "Roll- and pitch-plane coupled hydropneumatic suspension: Part 1: Feasibility analysis and suspension properties," *Vehicle Syst. Dyn.*, vol. 48, no. 3, pp. 361–386, 2010.

[10] D. Cao, S. Rakheja, and C.-Y. Su, "Roll- and pitch-plane-coupled hydropneumatic suspension. Part 2: Dynamic response analyses," *Vehicle Syst. Dyn.*, vol. 48, no. 4, pp. 507–528, 2010.

[11] F. Ding, X. Han, Z. Luo, and N. Zhang, "Modelling and characteristic analysis of tri-axle trucks with hydraulically interconnected suspensions," *Vehicle Syst. Dyn.*, vol. 50, no. 12, pp. 1877–1904, Jun. 2012.

[12] F. Ding, X. Han, N. Zhang, and Z. Luo, "Characteristic analysis of pitch-resistant hydraulically interconnected suspensions for two-axle vehicles," *J. Vib. Control*, vol. 21, pp. 1–22, Mar. 2014.

[13] J. Zhang, Y. Deng, N. Zhang, B. Zhang, H. Qi, and M. Zheng, "Vibration performance analysis of a mining vehicle with bounce and pitch tuned hydraulically interconnected suspension," *Chin. J. Mech. Eng.*, vol. 32, p. 5, Dec. 2019.

[14] Y. Wu, N. Zhang, B. Zhang, and J. Zhang, "Modeling and performance analysis of a vehicle with kinetic dynamic suspension system," *Proc. Inst. Mech. Eng. D, J. Automobile Eng.*, vol. 233, pp. 697–709, Jan. 2019.

[15] Q. Liu, N. Zhang, F. Feng, and M. Zhou, "Handling performance of tractor-semitrailers equipped with hydraulically interconnected suspension," *Proc. Inst. Mech. Eng. D, J. Automobile Eng.*, to be published. doi: 10.1177/0954407018817629.

[16] H. Qi, B. Zhang, N. Zhang, M. Zheng, and Y. Chen, "Enhanced lateral and roll stability study for a two-axle bus via hydraulically interconnected suspension tuning," *SAE Int. J. Vehicle Dyn., Stability, NVH*, vol. 3, no. 1, pp. 5–17, 2019.

[17] B. Tan, Y. Wu, N. Zhang, B. Zhang, and Y. Chen, "Improvement of ride quality for patient lying in ambulance with a new hydro-pneumatic suspension," *Adv. Mech. Eng.*, vol. 11, pp. 1–20, Apr. 2019.

[18] Z. Yin, A. Khajepour, D. Cao, B. Ebrahimi, and K. Guo, "A new pneumatic suspension system with independent stiffness and ride height tuning capabilities," *Vehicle Syst. Dyn*, vol. 50, no. 12, pp. 1735–1746, 2012.

[19] Z. Zhu, W. Gong, L. Wang, Q. Li, Y. Bai, and Z. Yu, "An efficient multi-time-step method for train-track-bridge interaction," *Comput. Struct.*, vol. 196, pp. 36–48, 2018.

[20] Z. Zhu, W. Gong, L. Wang, Y. Bai, Z. Yu, and L. Zhang, "Efficient assessment of 3D train-track-bridge interaction combining multi-time-step method and moving track technique," *Eng. Struct.*, vol. 183, pp. 290–302, Jan. 2019.

[21] M. Zheng, P. Peng, B. Zhang, N. Zhang, L. Wang, and Y. Chen, "A new physical parameter identification method for two-axis on-road vehicles: Simulation and experiment," *Shock Vib.*, vol. 2015, Jun. 2015, Art. no. 191050.

[22] L. Kong, M. Ostadhassan, C. Li, and N. Tamimi, "Pore characterization of 3D-printed gypsum rocks: A comprehensive approach," *J. Mater. Sci.*, vol. 53, pp. 5063–5078, Apr. 2018.

[23] Z. Guo, L. Peng, K. Feng, and W. Liu, "Measurement and prediction of nonlinear dynamics of a gas foil bearing supported rigid rotor system," *Measurement*, vol. 121, pp. 205–217, Jun. 2018.

[24] J. Dong, M. Chen, Y. Li, S. Wang, C. Zeng, and M. Zaman, "Experimental and theoretical study on dynamic hydraulic fracture," *Energies*, vol. 12, p. 397, Jan. 2019.

[25] W. Liu, K. Feng, Y. Huo, and Z. Guo, "Measurements of the rotordynamic response of a rotor supported on porous type gas bearing," *J. Eng. Gas Turbines Power*, vol. 140, Jun. 2018, Art. no. 102501.

[26] J. Dong, M. Chen, Y. Jin, G. Hong, M. Zaman, and Y. Li, "Study on micro-scale properties of cohesive zone in shale," *Int. J. Solids Struct.*, vol. 163, pp. 178–193, May 2019.

[27] S. Liu and K.-T. Wan, "A preliminary two-dimensional palpation mechanics for detecting a hard inclusion by indentation of a soft matrix under large strain," *J. Appl. Mech.*, vol. 86, no. 5, 2019, Art. no. 051009.

[28] Q. Tang, C. Du, J. Hu, X. Wang, and T. Yu, "Surface rust detection using ultrasonic waves in a cylindrical geometry by finite element simulation," *Infrastructures*, vol. 3, no. 3, p. 29, 2018.

[29] Q. Chen, A. Alizadeh, W. Xie, X. Wang, V. Champagne, J.-H. Lee, S. Müftü, and A. Gouldstone, "High-strain-rate material behavior and adiabatic material instability in impact of micron-scale Al-6061 particles," *J. Thermal Spray Technol.*, vol. 27, no. 4, pp. 641–653, 2018.

[30] Z. Zhang, C. Sun, R. Bridgelall, and M. Sun, "Application of a machine learning method to evaluate road roughness from connected vehicles," *J. Transp. Eng. B, Pavements*, vol. 144, 2018, Art. no. 04018043.

[31] Z. Zhang, C. Sun, R. Bridgelall, and M. Sun, "Road profile reconstruction using connected vehicle responses and wavelet analysis," *J. Terramechanics*, vol. 80, pp. 21–30, Dec. 2018.

[32] J. Tao and J. Hu, "Energy harvesting from pavement via polyvinylidene fluoride: Hybrid piezo-pyroelectric effects," *J. Zhejiang Univ.-Sci. A*, vol. 17, no. 7, pp. 502–511, 2016.

[33] B. Qiao, Z. Mao, J. Liu, Z. Zhao, and X. Chen, "Group sparse regularization for impact force identification in time domain," *J. Sound Vib.*, vol. 445, pp. 44–63, Apr. 2019.

[34] X. Sun, J. Liu, X. Han, C. Jiang, and R. Chen, "A new improved regularization method for dynamic load identification," *Inverse Problems Sci. Eng.*, vol. 22, no. 7, pp. 1062–1076, 2014

[35] Y. Chen, P. Logan, P. Avitabile, and J. Dodson, "Non-model based expansion from limited points to an augmented set of points using chebyshev polynomials," *Exp. Techn.*, pp. 1–23, Feb. 2019.

[36] C. Dong, X. W. Ye, and T. Jin, "Identification of structural dynamic characteristics based on machine vision technology," *Measurement*, vol. 126, pp. 405–416, Oct. 2018.

[37] S. Zhu, H. Du, N. Zhang, and L. Wang, "Development of a new model for roll-plane active hydraulically interconnected suspension," *SAE Int. J. Passenger Cars-Mech. Syst.*, vol. 7, no. 2, pp. 447–457, 2014.

[38] J. Zhou, X. Guo, C. Du, C. Cao, and X. Wang, "A fiber optic ultrasonic sensing system for high temperature monitoring using optically generated ultrasonic waves," *Sensors*, vol. 19, no. 2, p. 404, 2019.

[39] X. Guo, J. Zhou, C. Du, and X. Wang, "Highly sensitive miniature all-silica fiber tip Fabry–Pérot pressure sensor," *IEEE Photon. Technol. Lett.*, vol. 31, no. 9, pp. 689–692, May 1, 2019.

MING WANG received the B.E. degree from Hunan University, Changsha, China, in 2008, where he is currently pursuing the Ph.D. degree in mechanical engineering with the State Key Laboratory of Advanced Design and Manufacture for Vehicle Body. His current research interests include vehicle system dynamics and control, and shift control of transmission for electric vehicle.

BANGJI ZHANG received the B.E. degree from Jilin University, Changchun, China, in 1992, and the M.E. and Ph.D. degrees from Hunan University, Changsha, China, in 1999 and 2010,respectively, all in mechanical engineering. He was a Visiting Scholar with the University of Technology Sydney, Ultimo, NSW, Australia, from 2013 to 2014. He is currently a Professor with the College of Mechanical and Vehicle Engineering, Hunan University, and a Research Fellow with the State Key Laboratory of Advanced Design and Manufacturing for Vehicle Body.

YUANCHANG CHEN received the Ph.D. degree in mechanical engineering from the University of Massachusetts at Lowell, USA, in 2019. His research interests include vibration, structural dynamics, acoustics, signal processing, modal analysis, finite element analysis, vehicle system dynamics, and modal parameter identification. He is currently a member of the Society of Automotive Engineers (SAE), the American Society of Mechanical Engineers (ASME), and the Society for Experimental Mechanics (SEM).

NONG ZHANG received the B.E. degree from Northeastern University, Shenyang, China, in 1982, the M.E. degree from Shanghai Jiao Tong University, Shanghai, China, in 1984, and the Ph.D. degree from The University of Tokyo, Tokyo, Japan, in 1989, all in mechanical engineering.

He worked with several prestigious universities in China, Japan, USA, and Australia before joining the Faculty of Engineering and Information Technology, University of Technology Sydney, Ultimo, NSW, Australia, in 1995. He is currently a Professor with the School of Automotive and Transportation Engineering, Hefei University of Technology. His research interests include dynamics and control of automotive systems, including powertrains with various types of transmissions, hybrid propulsion systems for HEVs, vehicle dynamics, passive and active suspensions, and mechanical vibration, including experimental modal analysis, rotor dynamics, and cold rolling mill chatter.

JIE ZHANG received the Ph.D. degrees from Hunan University, Changsha, China, in 2018, where he is currently a Postdoctoral Researcher. His current research interests include control, modeling, and estimation of driver-vehicle system dynamics.